Transient and Dynamic Analysis of a Line-Start Radial Synchronous Reluctance Motor with Auxiliary Capacitive Winding

M. Muteba*
Department of Electrical Engineering Technology, University of Johannesburg, South Africa
*corresponding author's email: mmuteba@uj.ac.za

Abstract – *This paper deals with transient and dynamic analysis of a line-start radial synchronous reluctance motor (LSR-SynRM) with auxiliary stator capacitive winding (ASCW) suitable for direct drive industrial loads such as conveyor belts and centrifugal pumps. The machine which has been designed from an IE2-132S4 conventional foot mounted three-phase induction motor NEMA* frame *is modelled using Finite Element Method (FEM), then prototyped and tested for transient and dynamic capabilities. The stator slots house both main and auxiliary windings. The rotor laminations have two flux barriers, two radial magnetic ribs and four tangential magnetic bridges per pole. The upper and lower flux barriers accommodate copper bars, which are short circuited by common end rings. The time step Finite Element Model (FEM) coupled to an external capacitive circuit is utilized to analyze the transient behavior of the LSR-SynRM. To validate the numerical method, a testbed is set up for experimental measurements. The measured results evidenced that for any given capacitance value connected to the auxiliary winding, the LSR-SynRM successfully pulled into synchronism when started with no-load and with light load up to 25% of the full load. The results further proved that the LSR-SynRM with ASCW may be started at no-load or light load, and successfully be fully loaded after it has reached the synchronous speed and still be able to meet the IE4 efficiency, while operating with an excellent power factor.*

Keywords*: auxiliary winding, good power factor and efficiency, line-start synchronous reluctance motor, transient and dynamic analysis*

Article History
Received 5 July 2022
Received in revised form 15 January 2023
Accepted 14 February 2023

I. Introduction

Nowadays, most of the industrial applications which require high reliability, ease of maintenance and simplicity are driven by line-start Induction Motors (IMs). The use of efficient electric drives systems is inevitably sought as the international standards for the minimum energy efficiency of electrical machines are tightening [1]-[2]. The LSR-SynRM can achieve higher efficiency than its corresponding IM due to lack of rotor copper losses in steady state [3]-[4]. The LSR-SynRM can either be designed with squirrel cage like IM rotors and flux barriers placed below the cage bars, or by filling the flux barriers with conducting bars [3]. The latter provides good synchronization due to high reluctance torque compared with the case of separate squirrel cage [3]. The presence of rotor slots in LSR-SynRM with separate squirrel cage may increase torque pulsations due to space harmonic in the airgap magnetic conductance introduced by the slot openings. Although, LSR-SynRMs designed with high saliency ratio may enhance the power factor, but they barely achieved the power factor of their counterpart IMs. To improve the power factor of LSR-SynRMs to a competitive level, the use of auxiliary stator capacitive winding was suggested in [5].

The dynamic model of a line-start synchronous motor with auxiliary reactive compensation winding was presented in [6]. The authors in [5] and [6] mostly focused on the dynamic model and transient simulations of salient pole line-start synchronous motor with auxiliary reactive compensation. Practical measurements and analysis that elaborate on the effect of auxiliary stator capacitive winding and mechanical load on the transient and dynamic capabilities of a line-start synchronous motor with auxiliary reactive compensation winding that meets the IE4 efficiency have not yet been reported. This paper presents new results and analysis that focused on the effect of capacitance value and mechanical load on transient and dynamic capabilities of a three-phase LSR-SynRM with ASCW. The results further ascertain that the LSR-SynRM is a strong contender to the IM in industrial direct drive motors that require high efficiency and excellent power

factor and may start with no or light mechanical load. This paper is organized along these lines: section II reports on the ratings and specifications of the LSR-SynRM with ACSW. Section III discusses the effect of number of rotor bars in the LSR-SynRM and squirrel cage IM. The time step finite element analysis (FEA) for ac transient solution is discussed in section IV. The testbed set up is introduced in section V, while section VI reports on the transient and dynamic analysis of the LSR-SynRM with ACSW. The analysis of performance behavior under steady state operation is reported in section VII. Key findings of this paper are summarized in section VIII.

II. Ratings and Specifications

The rotor of the LSR-SynRM presented in this article has copper bars which are inserted into the flux barriers as shown in Fig. 1(c) and (d). The upper flux barriers accommodate eight bars of 10 mm x 10 mm each, while the lower flux barriers accommodate eight bars of 16 mm x 12 mm each. Neglecting the end-ring connection, the lower and upper bars have equivalent resistance of 0.231 x 10^{-3} Ω and 6.935 x 10^{-3} Ω at 20 ^{O}C, respectively. The LSR-SynRM starts and accelerates mainly due to asynchronous torque. The current in rotor copper bars falls to zero when the rotor field aligns with the stator magnetic field to produce a reluctance torque at synchronous speed. Fig. 1(a) shows the prototype stator with dual winding, while Fig. 1(b) shows the rotor of the IE2-132S4 conventional three-phase IM. On the other hand, Fig. 2 illustrates on the motor's topology and connection diagram. Key ratings and specifications of the LSR-SynRM with ASCW are given in Table I. The rotor of the IE2-132S4 conventional three-phase IM shown in Fig. 1(b) has 43 rotor bars skewed by one stator slot pitch.

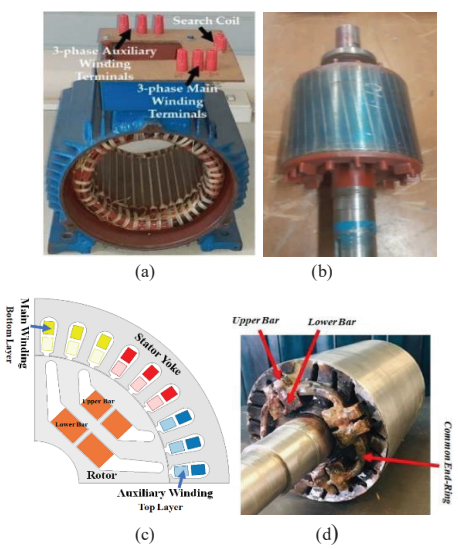

Fig.1. (a) Prototype stator with dual windings, (b) rotor of the IE2-132S4 three-phase IM, (b) proposed LSR-SynRM's 2D cross section: - a pole view, (d) proposed LSR-SynRM's prototype rotor

TABLE I
RATINGS AND SPECIFICATIONS FOR THE PROTOTYPE LRS-SYNRM

Description	Unit	values
Stator external diameter	*mm*	210
Stator bore diameter	mm	150
Rotor external diameter	mm	149.3
Core length	mm	160
Airgap length	mm	0.35
Pole pairs	-	2
Frequency	Hz	50
Rated current main winding	A	13.88
Rated current auxiliary winding	A	6.5
Slot fill factor main winding	%	33.08
Slot fill factor auxiliary winding	%	9.33
Current density	A/mm^2	5.68
Number of stator slots	-	36
Number of upper rotor bars	-	8
Number of lower rotor bars	-	8
Turns per coil main/auxiliary	-	18/18

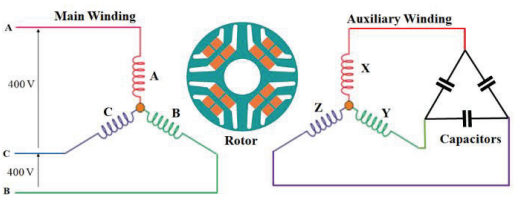

Fig. 2. Line-start radial synchronous motor's topology and connection diagram

III. Effect of Number of Rotor Bars

A. *Presence of field harmonics in* squirrel cage IM and *LSR-SynRM*

The rotor bar current induces a magnetic field with a certain number of harmonic components. The field rotor harmonic orders are found by using the following [11]-[12],

$$v_r = x\frac{N_b}{p_1} + 1 \qquad (1)$$

where x is any integer positive or negative number, N_b is the number of rotor bars, and p_1 is the number of fundamental pairs of poles. The rotor of the IE2-132S4 conventional three-phase IM, beside the fundamental component, produces during transient and steady-state operations, odd and even space harmonics of order -20 or -21, +22 or +23, -42, +44 and so on. In contrast, the rotor of the proposed LSR-SynRM, which produce only during transient operation, odd space harmonics of order -3, +5, -7, +9, -11, +13 etcetera. The two machines have the same stator NEMA frame and the same winding configuration. Therefore, the space harmonics produced by the stator slotting and the stator main, and auxiliary windings phase-belts are the same in both machines, and they can be obtained as in (2) and (3) respectively [11]-[12].

$$v_s = x\left(\frac{N_s}{p_1}\right) + 1 \quad (2)$$

$$u_s = 2x\left(\frac{\pi}{\beta}\right) + 1 \quad (3)$$

Here N_s is the total number of stator slots, β is the phase belt angle, which is π/3 electric radian for a 36-stator slot, 3-phase, and 4-pole machine. The LSR-SynRM with ASCW and the squirrel cage IM, beside the fundamental, produce stator slot space harmonics of order -17 , +19, -35, +37 etcetera and the phase-belt space harmonics of order -5, +7, -11, +13, -17, +19, -23, +25, -29, +31, -35, +37 and so on. The field harmonics with a positive sign are moving in the same direction as the fundamental component and those with a negative sign are traveling in the opposite direction [12]. It should be noted that the auxiliary winding, once energized by capacitors, it also produces stator slot and phase belt space harmonic having the same order numbers as the main winding's field harmonics.

B. *Existence of Parasitic Torques*

The field harmonic components derived from the rotor give rise to synchronous parasitic torques when interacting with the field harmonics emanated from the stator with the same order [12]-[13]. The interaction of the rotor slot field harmonics and stator winding phase belt harmonics are shown in Table II.

TABLE II
INTERACTION OF FIELD HARMONICS

LSR-SynRM	IM	Interaction	Interaction
Rotor Harmonics	Rotor Harmonics	Stator Phase-Belt Harmonics	Stator Slot harmonic
+5	-	-5	-17
-7	-	+7	+19
-11	-	+11	-35
+13	-	+13	+37
+17	-	-17	-53
-19	-	+19	+55
-23	+23	-23	-71
+25	-	+25	+73

From Table II, it is noted that in the LSR-SynRM, all the rotor slot field harmonics that are not multiples of three, interact during starting and cancelation periods with the stator winding phase belt harmonics, thus causing synchronous parasitic torques at sub-synchronous speeds. On other hand, only the 23rd rotor bars harmonic order and the 23rd stator winding phase belt harmonic order interrelate in the squirrel cage IM. Another observation from Table II is that there is no interactivity between the rotor slot harmonic and the stator slot harmonic in the squirrel cage IM, but this is not the case for the LSR-SynRM. In the later, the 5th rotor slot harmonic (17th order) interlinks with the 1st stator slot harmonic (17th), and they bring about synchronous parasitic torque at a certain sub-synchronous speed. The same is observed for the 19th, 35th, 37th, etcetera. A fair comparison between the squirrel cage IM and the proposed LSR-SynRM on transient performance cannot be undertaken in this article. The squirrel cage IM has an advantage over the LSR-SynRM because of its adequate number of stator slot and rotor bar combination. For a 4-pole, 36-slot machine with a skewed rotor, the stator slot and rotor bar combinations should be 36/25, 36/27, 36/28, 36/29, 36/30 and 36/43 [12]. For fair comparison on transient performance, both motors should have the same number of rotor bars as it is the case in [14].

IV. Finite Element Analysis

A two-dimensional (2D) FEA is performed using the Maxwell ANSYS Electronics Desktop 2021R1 electromagnetic package. The full-pitched three-phase main windings are excited by 3-phase sinusoidal voltage. The three-phase auxiliary windings are coupled to an external circuit having capacitors as shown in Fig. 3. Fig. 4(a) to (d) show the effect of capacitance value on the flux density distribution in the iron core of the LSR-SynRM. Moreover, Fig. 5(a) to (d) show the no-load transient currents for the LSR-SynRM with ASCW.

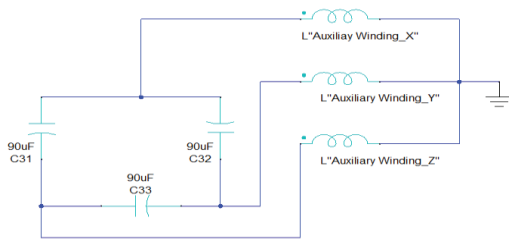

Fig.3. Maxwell circuit of the three-phase auxiliary windings coupled to external capacitive circuit

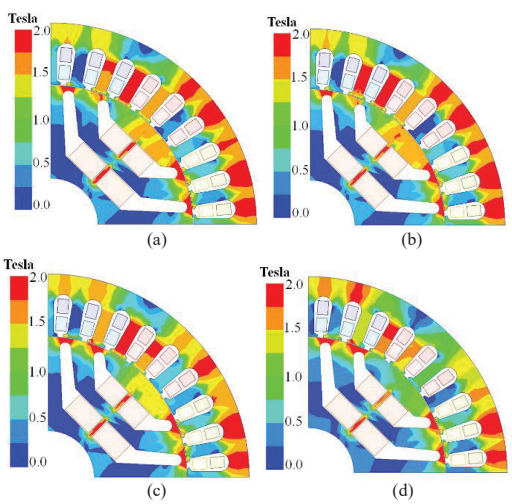

Fig.4. Flux density distribution on no-load, (a) 0 µF (b) 90 µF (c) 120 µF, (d) 160 µF

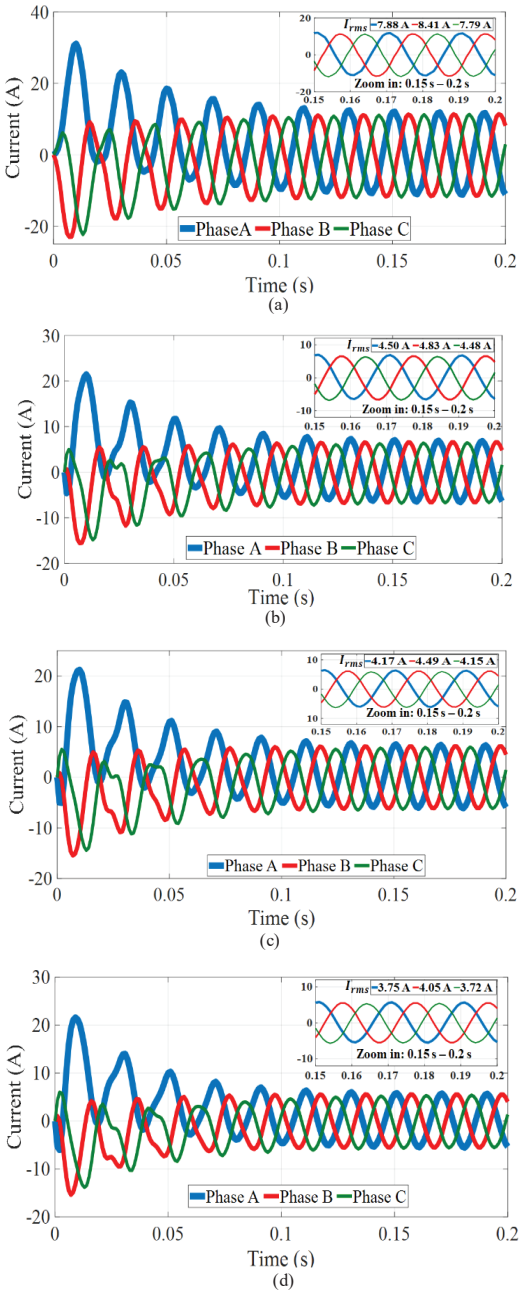

Fig. 5. Starting three-phase current at no-load, (a) 0 µF (b) 90 µF (c) 120 µF, (d) 160 µF

Although the core losses are considered in the model, the skin effects are disregarded in the FEA for ac magnetic-transient solution. Due to the symmetry of the motor, only a pole-pitch is considered in the FEA. The flux density distribution plots were obtained at locked rotor, and they lie in the plane of the model (x, y). The vector boundary condition with zero vector potential was set to the outer region of the machine's model. The edges of the 2D Cartesian-coordinate area were modelled with Master boundary condition on the x-axis and Slave boundary condition on the y-axis. A total number of 1868 elements were obtained for the one-pole pitch machine's geometry. Element Length Based mesh operation was applied on the rotor core and stator core geometries with minimum edge length of 0.0005 mm and 0.00085 mm respectively, and a maximum edge length of 0.0235 mm and 0.0103 mm respectively. Moreover, the Surface Approximation mesh operation was applied on the phase coil and rotor bar geometries. The coils had a minimum and maximum edge lengths of 0.00206 mm and 0.0052 mm respectively. Each upper rotor bar had a minimum and maximum edge lengths of 0.0023 mm 0.0125 mm respectively. On the other hand, each lower rotor bar had a minimum and maximum edge lengths of 0.0048 mm 0.0202 mm respectively. The simulation's stop time and time-step size were 0.2 sec and 0.001 sec respectively.

From Fig. 4, it is noted that the localized magnetic saturation on the stator back iron reduces with the increase in capacitance value. This is due to the decrease in magnetizing current that causes the magnetic saturation to also descrease wth the increase in capacitance value [9].

The effect of capacitance value is noticeable on the transient current characteristics of the LSR-SynRM with ASCW. With no-capacitance in the auxiliary winding, the rms steady-state current in phase *B* on no-load is about 8.41A. With a 90μF per phase connected to auxiliary winding, the rms steady-state current in phase *B* on no-load drops to 4.83 A. The trend continues when larger capacitance values are connected to the auxiliary winding. With capacitance values of 120μF and 160μF per phase, the rms steady-state currents in phase *B* on no-load are 4.49 A and 4.05 A respectively. The FEA results in Fig. 5 (a) to (d) evidenced that starting and the steady state rms values of current in the main windings decrease with an increase in auxiliary capacitance value. It should be noted that the maximum required capacitance value is dictated by the permissible maximum current that the auxiliary winding may carry without overheating and the permissible magnetic saturation level in the magnetic core of the machine.

V. Experimental Set-Up

A 7.5 kW induction motor fed from a Siemens SINAMICS four-quadrant energy recovery ac drive was employed to load the LSR-SynRM with ASCW, and a DR-3000-P type torque sensor with the range from 0 to 200 Nm was utilized to measure the mechanical power, speed, and torque of the rotating shaft. Signal output is transmitted directly from the shaft to a PC through a USB interface. Fig. 6 shows the experimental setup rig photo.

The Dranetz PowerVisa 4400 three-phase power analyzer, equipped with eight independent channels, was made use to measure the voltage, current, input power and power factor, and the Hantek DSO4004C Series six channels digital oscilloscope was employed to store and analyze the voltage and current waveforms. The start and

stop operations of the LSR-SynRM was made possible by start and stop buttons incorporated in a motor controller. A variable ac power supply was used to vary the motor voltage during no-load and locked rotor tests. Fixed capacitors arranged in delta configuration, were connected either in series or parallel to provide different capacitance values.

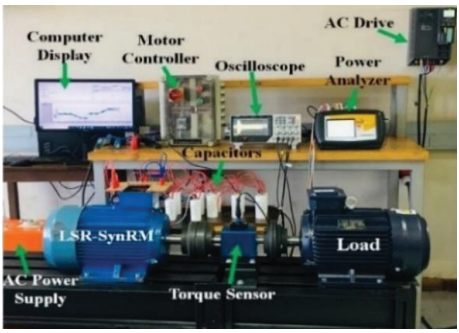

Fig. 6. Experimental setup rig photo

To determine the magnetizing inductance, the machines was fed at rated frequency and rated voltage with the load removed from the shaft. The rotor dc resistance and total leakage inductance referred to the stator main winding were determined using the locked rotor test, while the stator main and auxiliary winding resistances were determined using the conventional dc test. The per phase equivalent parameters of the LSR-SynRM without reactive compensation are depicted in Table III. It should be noted that the total leakage reactance and rotor resistance in Table III were referred to the stator main winding.

TABLE III
EQUIVALENT PARAMETERS OF THE LSR-SYNRM

Description	Unit	values
Resistance of main winding	Ω	0.6
Resistance of auxiliary winding	Ω	2.12
Total leakage reactance	Ω	8.16
Rotor resistance	Ω	0.583
Core loss resistance	Ω	101.7
Magnetizing reactance	Ω	24.49

VI. Transient and Dynamic Analysis

A. Effect of Capacitive Winding on Synchronization Capability

Fig. 7(a) to (d) show the effect of capacitance value and mechanical load on the starting and synchronization capabilities of the LSR-SynRM with ASCW. The experimental measurements were conducted at name plate voltage and frequency of 380 V and 50Hz, respectively. At starting, the frequency of the rotor current is high and equal to the frequency of the supply. The current amplitude is distributed between the upper and lower cage bars in inverse proportion to their impedances. Since the lower cage bars have high leakage inductive reactance at starting, and their equivalent impedance is many times that of the upper cage bars, the current in the lower cage bars is smaller than that in the upper cage bars. The torque during starting is developed mainly by the current flowing through the upper cage bars. As the LSR-SynRM with ASCW starts to accelerate, the frequency of the rotor current starts to decrease, this results in the reduction of the rotor leakage inductive reactance, and an augmentation of current in the lower cage bars.

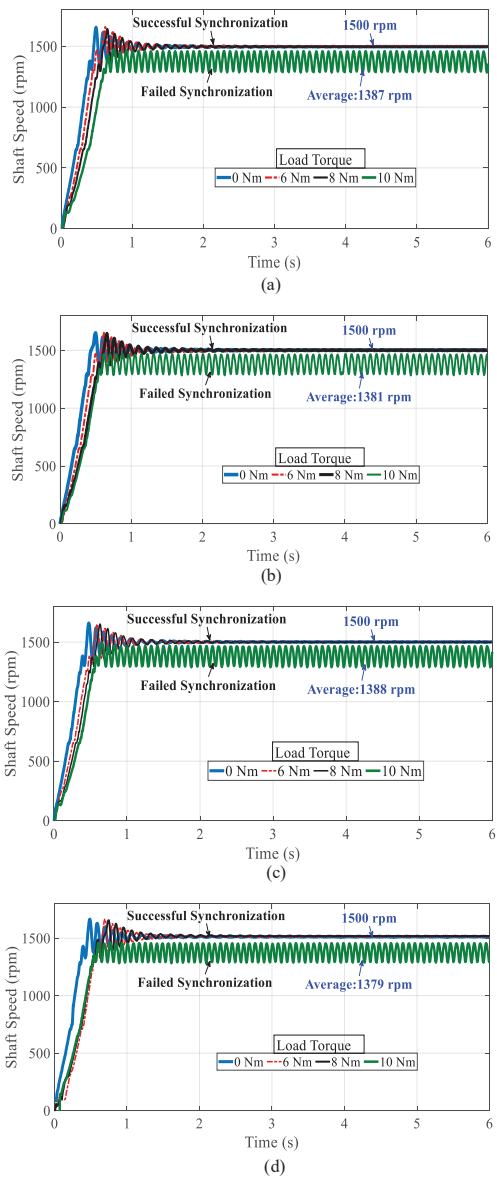

Fig.7. Speed of RLS-SynRM at start-up with different mechanical loads, (a) 0 µF (b) 90 µF (c) 120 µF, (d) 160 µF

Consequently, the acceleration torque is mainly developed by the current flowing through the lower cage bars. The total starting and accelerating currents of the whole rotor cage bars are divided between the upper and lower cage bars in inverse proportion to their resistances, and, since the equivalent resistance of upper cage bars is almost thirty times the equivalent resistance of the lower cage bars, the current in the upper cage bars becomes smaller than that in the lower cage bars. The rotor current falls to zero at synchronous speed, and the LSR-SynRM with ASCW develops only reluctance torque.

It is noted from the experimental results in Fig. 7(a) to (d) that there is failed synchronization when the LSR-SynRMs started with a load torque of 10 Nm, which corresponds to 30% of the full load. With failed synchronization, the LSR-SynRM with ASCW operates at steady-state as an induction motor with a slip of ± 7.5%. For successful synchronization and for any given value of capacitance, the time duration from start to steady-state is ± 1sec. The effect of capacitance value is not significant on the synchronization capability of the LSR-SynRM with ASCW.

B. Effect of Capacitive Winding on Starting and steady-state Currents

Fig. 8(a) to (d) depict the measured transient currents on no-load for different values of capacitance values. Although the effect of capacitance value was not significant on the synchronization capability of the LSR-SynRM with ASCW, it was well noted on the starting and steady-state current characteristics as shown in Fig. 8(a) to (d). It was well established in [9] that when there is no capacitor connected to the auxiliary winding of an IM, the current in the auxiliary winding is zero. Its flux linkage is also zero, therefore making the mutual reactance between the main and auxiliary windings inexistant. The no-load current is totally magnetizing, and the magnetizing reactance is dependent only on the inverse airgap length [9]. When the no-load current increases, the magnetic saturation factor increases, so the magnetizing reactance decreases. Both the airgap length and saturation factor have an effect on the magnetizing reactance [9]. Once a set of capacitors is connected to the auxiliary winding, an excitation current will flow through it. In this case, there is a flux linkage associated with the auxiliary winding. A common mutual reactance occurs due to the mutual coupling of the main and auxiliary windings non-airgap flux components (leakage flux) [15]. The presence of capacitors in the auxiliary winding increases the magnetizing reactance, while decreasing the no-load and magnetizing currents, thus improving the power factor [9].

The measured results in Fig. 8 show that with no-capacitance in the auxiliary winding, the rms values of the starting and steady-state currents on no-load are about 37.7A and 9.2A respectively. A no-load steady-state current of 9.2A for a motor having a rated current of 13.88 A is quite high. The LSR-SynRM requires a huge amount of magnetizing current to develop the necessary reluctance torque. The starting current drops by 15% and the steady-state current by 38% when a capacitor of 90 µF per phase

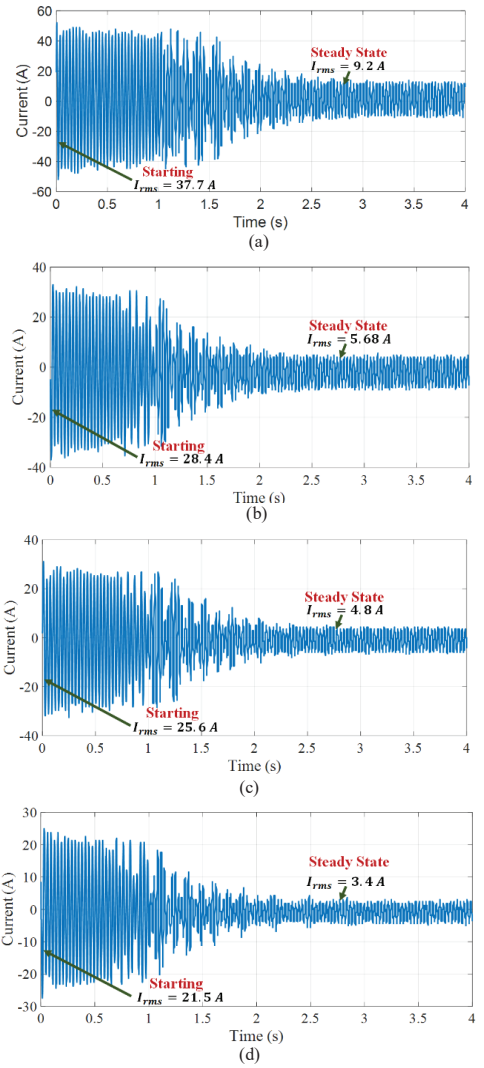

Fig.8. Starting current characteristics on no-load, (a) 0 µF (b) 90 µF (c) 120 µF, (d) 160 µF

is connected to auxiliary winding. With a capacitor of 120 µF per phase connected to auxiliary winding, the starting current drops by 32% and the steady-state current by 48%. The starting current drops by 43% and the steady-state current by 63% with a capacitor of 160 µF connected to the auxiliary winding. The LSR-SynRM with the highest capacitance value has achieved very low starting and steady-state currents. The decrease in starting and steady state currents when the capacitance value increases was also noted in FEA results reported is Section III of this paper. The results from experimental measurements corroborated the results from numerical method.

C. Analysis of Dynamic Responses

This subsection deals with transients related to dynamic responses when the LSR-SynRM with ASCW is synchronized and the mechanical load, is gradually changed. The dynamic responses for shaft torque of the LSR-SynRM with different capacitance values connected to auxiliary winding are shown in Fig. 9(a) to (d).

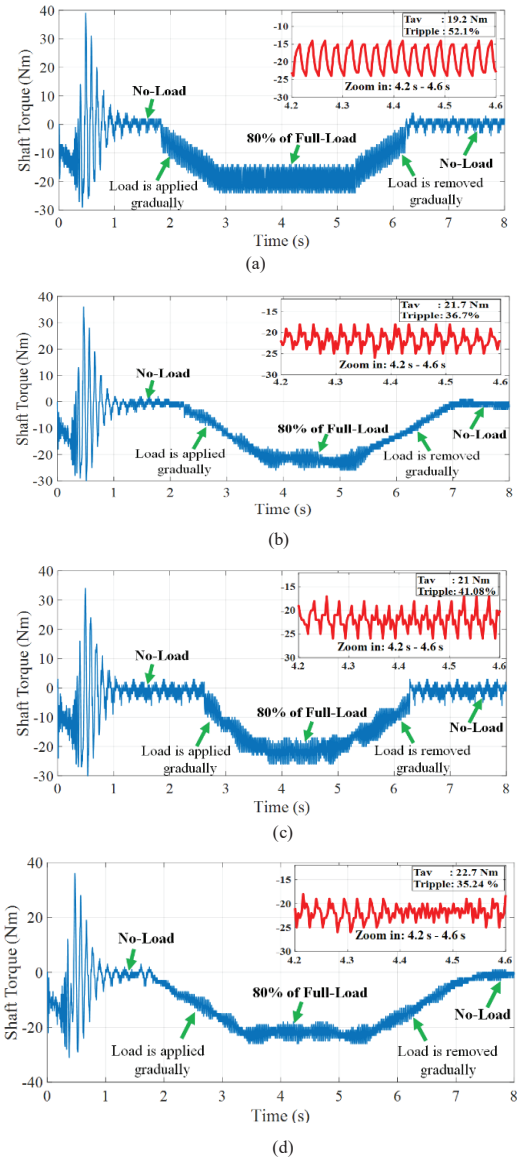

Fig.9. Dynamic responses: -torque characteristics, (a) 0 µF (b) 90 µF (c) 120 µF, (d) 160 µF

In Fig. 9(a), the mechanical load is gradually applied from 1.75sec until 80% of the full load is attained at 3sec, and the load is kept constant for about 2.3sec before it is gradually removed. Elsewhere in in Fig. 9 (b), the mechanical load is gradually applied from 2.6sec until 80% of the full load is attained at 3.8sec, and the load is kept constant for about 2.4sec before it is gradually removed. In Fig .9 (c) and (d), the loads are applied at 2.6sec and 1.7sec respectively, and they are kept constant for about 1.6sec and 2sec respectively.

The time responses from no-load to 80% of the full load are 1.25sec, 1.2sec, 0.7sec and 1.5sec for 0 μF, 90μF, 120μF and 160μF, respectively. On the other hand, the time responses from 80% of full load to no-load are 1sec, 1.7sec, 1.5sec and 2sec for 0 μF, 90μF, 120μF and 160μF, respectively. The attendance of capacitors in the auxiliary winding circuit has compensated the LSR-SynRM's magnetizing capability. The motor does not need to draw more magnetizing current from the power grid to develop the same amount of torque. The effect of capacitance value is also noticed in the LSR-SynRMs' time responses. An optimal value of auxiliary capacitive winding is required for a minimum time response. This can be achieved by means of an appropriate design optimization approach, which is not the scope of this paper. The measured results in Fig. 9 (a) to (d) evidenced that the torque quality is also influenced by the capacitance value in the auxiliary circuit.

With 80% of full load connected to the shaft, the torque ripples are 52.1%, 36.7%, 41.08% and 35.24% for capacitance values of 0 μF, 90μF, 120μF and 160μF, respectively. The torque ripple is high when the LSR-SynRM operates with zero value of capacitor in the auxiliary. The torque ripple drops when capacitors are introduced in the auxiliary winding. The pattern in torque ripple drop is not uniform. The machine with 120μF capacitor has high torque ripple than the machine with a capacitor value of 90μF. Therefore, an optimization approach is required to obtain the optimal value of capacitors that will provide fast dynamic response and minimum torque ripple during steady state operation.

VII. Performance Under Steady-State Operation

The comparison of performance indexes is depicted in Tables IV and V. It should be noted that the experimental results in Tables IV and V were obtained under steady state condition. The current in the rotor cage bars is zero, and the rotor copper losses are also zero. Only the stator winding losses exist. In this paper, the skin effects are not considered in the analysis, and the winding ac losses are disregarded. From the results in Tables IV and V, it is evident that the capacitance value had an impact on both the main and auxiliary winding copper losses. Although the current flowing in the auxiliary winding is totally magnetizing, but it produced heat due to joules losses as these losses depend on the magnitude of the current and not on its phase angle.

The efficiency was determined indirectly according to the IEC 60034-2-1 standard test method 2-1-1B by the summation of separate losses [7]-[8]. In this paper the test

was conducted at different load points between no-load and 80 % of the rated torque for nominal frequency of 50 Hz. The residual losses P_{RL} were determined for each load point by subtracting from the input power P_{in}, the output power P_{out} , the constant losses P_c, the stator primary (main) winding losses $P_{spCu} = \left(3I_{sp}^2 R_{sp}\right)$ and the stator auxiliary winding losses $P_{asCu} = (3I_{sa}^2 R_{sa})$ [9]. The residual and constant losses for the three-phase LSR-SynRM with auxiliary capacitive winding were determined using (4) and (5) respectively.

$$P_{RL} = P_{in} - P_{out} - P_c - 3\left[\left(I_{sp}^2 R_{sa}\right) + \left(I_{sa}^2 R_{sa}\right)\right] \quad (4)$$

$$P_c = P_0 - 3\left[\left(I_{sp0}^2 R_s\right) + \left(I_{sa}^2 R_{sa}\right)\right] \quad (5)$$

Where, P_{in} is the electrical input power and P_o is the steady state active power on no-load. The constant losses are defined using $\left(P_{rot} + P_{fe}\right)$, where P_{rot} and P_{fe} are the rotational and iron losses respectively. Here the constant losses were obtained at name plate voltage in contrast to induction motors where the constant losses were obtained for various terminal voltages [10]. In this paper, the LSR-SynRM is designed from a three-phase induction motor NEMA frame. Eq. (6) was used to obtain the rotational losses, which is generally used for conventional small and medium-sized induction motors [1].

$$P_{rot} = \left(\frac{3}{p}\right)^2 D_{ext}^4 \times 10^4 \quad (6)$$

In (6), D_{ext} represents the stator external diameter which value is given in Table I. The total losses are calculated using (7), and the efficiency at each of the load points is determined as in (8).

$$\sum losses = P_{fe} + P_{rot} + 3\left[\left(I_{sp}^2\, R_s\right) + \left(I_{sa}^2\, R_{sa}\right)\right] \quad (7)$$

$$Eff = \frac{P_{in} - \sum losses}{P_{in}} \quad (8)$$

TABLE IV
STEADY-STATE PERFORMANCE INDEXES AT NO-LOAD

Indexes	Unit	0 µF	90 µF	120 µF	160 µF
I_{sp}	A	9.2	5.7	4.8	3.4
I_{sa}	A	0	3.1	4.2	5.7
P_{spCu}	W	152.3	58.5	41.5	18.4
P_{saCu}	W	0	61.2	111.1	206.6
P_{fe}	W	150.4	175.1	183.2	194.9
P_{RL}	W	96.5	92.9	91.3	86.4
Eff	%	29.4	21.6	19.2	14.7
PF	-	0.199	0.564	0.715	0.774

Due to high flux density fluctuations mainly caused the rotor anisotropy, the iron losses are high compared to an induction motor of the same size. Under no-load operation, the efficiencies are very low, especially for the machine with the highest auxiliary capacitance value. This is due to high auxiliary winding copper and iron losses recorded on no-load. These losses increase when the auxiliary capacitance value increases. As expected, the LSR-SynRM with the highest auxiliary capacitance value has achieved better power factors of 0.774 and 0.922 lagging, on no-load and 80% of the full load respectively, and it has also met the IE4 efficiency at 80% of the full load, despite having high auxiliary winding copper losses and iron losses.

TABLE V
STEADY-STATE PERFORMANCE INDEXES AT 80 % OF FULL-LOAD

Indexes	Unit	0 µF	90 µF	120 µF	160 µF
I_{sp}	A	11.1	7.9	7.2	6.8
I_{sa}	A	0	3.1	4.2	5.7
P_{spCu}	W	221.8	112.2	93.3	83.2
P_{saCu}	W	0	61.2	111.1	206.6
P_{fe}	W	150.4	175.1	183.2	194.9
P_{RL}	W	106.8	99.21	97.4	94.2
Eff	%	82.5	83.2	83.9	85.1
PF	-	0.616	0.753	0.862	0.922

VIII. Conclusion

This paper analyzed the transient and dynamic performance of a line-start radial synchronous reluctance motor with auxiliary capacitive winding. The analysis was based on both finite element analysis and experimental measurements. The results evidenced that the presented motor is suitable in applications that may not require to start with a huge mechanical load, such as conveyor belts and centrifugal pumps. Not only the proposed motor has proved to have good starting and dynamic capabilities, but it has also reduced starting and steady state no-load, and load current compared to machine without auxiliary capacitive. The results further evidenced that the proposed motor can operate with very excellent power factor while achieving the IE4 efficiency. An optimization approach may be required to determine the optimal value of capacitors to be employed in the auxiliary winding. Future work may include to design the proposed motor with same number of rotor bars than its counterpart three-phase induction motor for fair comparison as far as transient and dynamic performances are concerned.

Acknowledgements

This work has been funded by the South African National Research Foundation (NRF) through the Thuthuka research grant framework under the emerging career researchers and scholars' tracks: www.nrf.ac.za

Conflict of Interest

The author declares no conflict of interest in the publication process of the research article.

References

[1] A.T.D Almeida, F.J.T.E Ferreira and G. Baoming, "Beyond Induction Motors-Technology Trends to Move Up Efficiency,"

IEEE Trans. On. Ind. Appl., vol. 50, No. 3, *p.p. 2103–2114, May/June 2014.*

[2] H. Kim, Y. Park, S.T. Oh, H. Jang, S.H Won, Y.D Chun and J.A. Lee, "Study on the Rotor Design of Line Start Synchronous Reluctance Motor for IE4 Efficiency and Improving Power Factor," *Energies., Vol.13*, No. 21:5774, *2020.*

[3] V. Abramenko, J. Bárta, I. Lolová, I. Petrov, and J. Pyrhönen, "Design of a Low-Power Direct-on-Line Synchronous Reluctance Motor Based on the Modified Natural Flux Line Curve Approach", *IEEE Trans. On. Ind. Appl., vol. 57*, No. 6, *pp. 5894–5906, Nov/Dec 2021.*

[4] G. A. Uvaraj, N.C. Lenin, S. Padmanabhan and B. Khan, "Line start synchronous reluctance motor with improved power factor for agriculture electric pump applications", *J. Eng., Vol.1.,* No.17., *Dec 2021.*

[5] A. M. Epemu, D U. Onyishi and E. Oboe, "Performance Analysis of Line-Start Concentrated Dual-winding Synchronous Reluctance Machine with Capacitive Assistance", *Journal of Science, Vol 35*, No 3, *p.p. 917-934, 2022.*

[6] A. S. O. Ogunjuyigbe, A. A. Jimoh and T.R. Ayodele, "Dynamic and transient behavior of a line start capacitance compensated synchronous reluctance machine", *Journal of Electrical Systems and Information Technology, vol. 4*, no. 3*, pp. 843-860, Dec. 2018.*

[7] IEC 60034-2-1: 2014, Rotating electrical machines - part 2-1: Standard methods for determining losses and efficiency from tests, IEC: Geneva, Switzerland, 2014.

[8] R.I. Rivera, J.C. Tálaga, R.M. Castrillón, E.C. Quispe, " Implementation of a Procedure to Determine Induction Motor Efficiency According to the IEC 60034-2-1 Standard". *In the proceedings of the IEEE ANDESCON, Santiago de Cali, Colombia, 22-24 August, 2018.*

[9] M. Muteba, "Optimization of Air Gap Length and Capacitive Auxiliary Winding in Three-Phase Induction Motors Based on Genetic Algorithm", *Energies*, Vol. 14, No. 15:4407, *2021.*

[10] S. Xiaobo, M. Dawei, Y. Xiaoni, "Influence of impeller's torque ripple on motor loss and efficiency of contra–rotating axial–flow fan", *Electric Machines and Control, Vol. 22*, p.p. 40–47, *2018.*

[11] M. Muteba, Comparison of dynamic behaviors between a synchronous reluctance motor with brass rotor bars and a squirrel cage induction motor, in IEEE PES/IAS PowerAfrica, Abuja, Nigeria, Aug 20-23, 2019, 10.1109/PowerAfrica.2019.8928746

[12] I. Boldea, S. A. Nasar, The induction machine handbook , CRC Press, New York, 2002.

[13] L. Wang, X. Bao, C. Di, Y. Zhou and Q. Lu, Analysis of synchronous parasitic torque in dual skew cage rotor induction motors with equivalent slot number, IET Elect. Power Appl., 2017, Vol. **11**(8), 1357-1365, 2017, 10.1049/iet-epa.2016.0565

[14] A. Kersten, Y. Liu, D. Pehrman and T. Thiringer, "Rotor Design of Line-Start Synchronous Reluctance Machine With Round Bars," in *IEEE Transactions on Industry Applications*, vol. 55, no. 4, pp. 3685-3696, July-Aug. 2019, doi: 10.1109/TIA.2019.2914010

[15] Muljadi, E.; Lipo, T.A.; Novotny, D.W. Power Factor Enhancement of Induction Machines by Means of Solid State Excitation. *IEEE Trans. Pow. Electr.,* 1989, *4*, 409-418.